Pressure-induced structural change of liquid InAs and the systematics of liquid III-V compounds

T. Hattori*
Synchrotron Radiation Research Center, Japan Atomic Energy Agency, Kouto, Sayo, Hyogo 679-5148, Japan

K. Tsuji
Department of Physics, Keio University, Hiyoshi, Yokohama 223-8522, Japan

Y. Miyata, T. Sugahara, and F. Shimojo
Department of Physics, Kumamoto University, Kumamoto 860-8555, Japan

(Received 17 July 2007; revised manuscript received 12 September 2007; published 30 October 2007)

To understand the pressure-induced structural changes of liquid III-V compounds systematically, the pressure dependence of *l*-InAs was investigated using the synchrotron x-ray diffraction and an *ab initio* molecular-dynamics simulation (AIMD). The x-ray diffraction experiments revealed that the liquid changes its compression behavior from a nearly uniform type to a nonuniform one around 9 GPa. Corresponding to this change, the coordination number (CN), which is maintained up to 9 GPa, markedly increases from 6.0 to 7.5. The AIMD simulation revealed that this change is related to the change in the pressure dependence of all three pair correlations. In particular, a marked change is observed in the As-As correlation; in the low-pressure region, the position of the first peak in $g_{\mathrm{AsAs}}(r)$, r_{AsAs}, increases while maintaining the $\mathrm{CN}_{\mathrm{AsAs}}$, but in the high-pressure region, the r_{AsAs} stops increasing and the $\mathrm{CN}_{\mathrm{AsAs}}$ begins to increase. The AIMD simulation also revealed that each partial structure of *l*-InAs is similar to that for the pure-element liquid with the same valence electron number. Upon compression, each partial structure approaches the respective one for a heavier element in the same group. These findings suggest that the structures of liquid compounds are locally controlled by the number of the valence electrons in each ion pair and that the change in each partial structure obeys the empirical rule that the high-pressure state resembles the ambient state of a heavier element in the same group. Comparing the pressure-induced structural change of *l*-InAs to those of other liquid III-V compounds (GaSb and InSb) has revealed that, although the high-pressure behaviors of these three liquids are apparently different, their structural changes are systematically understood by a common structural sequence. This systematics originates from the same effect on each partial structure between increasing the atomic number and the pressurization.

DOI: 10.1103/PhysRevB.76.144206 PACS number(s): 61.20.Qg, 61.10.Eq, 07.35.+k

I. INTRODUCTION

Recent developments in synchrotron radiation sources and high-pressure generation techniques open up opportunities to determine liquid structures precisely, and now, pressure-induced structural changes of many liquids are investigated. In particular, liquids of tetrahedrally bonded materials, such as Si, Ge, III-V, and II-VI compounds, have attracted much attention.[1–9] It is because these liquids retain a covalent chemical bonding nature even after metallization upon melting and likely show marked pressure-induced structural changes due to the reduction of the covalent nature at high pressures. Among them, the structural changes of liquid III-V compounds have been thoroughly investigated,[4,5,7] and the following features have been reported:

(i) Liquid GaSb (*l*-GaSb) contracts nonuniformly over a wide pressure region up to 20 GPa. Upon compression, the anisotropy in the local structure gradually decreases and the coordination number (CN) continuously increases. This can be understood by the continuous decrease of the covalent bonding nature upon compression.[4]

(ii) Liquid InSb (*l*-InSb) shows almost the same behavior up to 10 GPa, but at higher pressures, the liquid contracts almost uniformly. In the high-pressure region, the liquid maintains its coordination number and the shapes of the total structure factor $S(Q)$ and the total pair distribution function $g(r)$. This suggests the existence of a relatively stable liquid form above 10 GPa.[7]

(iii) In contrast to *l*-InSb, liquid InAs (*l*-InAs) changes its contraction behavior from a nearly uniform type to a nonuniform one around 9 GPa.[5] Corresponding to this change, the CN, which remains constant below 9 GPa, increases at higher pressures.

Although all these liquids commonly belong to the III-V compounds family, they show apparently different contraction behaviors. To reveal its nature, this study investigated the pressure dependence of the structure of *l*-InAs and compared the results to those of *l*-GaSb and *l*-InSb. Although the pressure dependence of the structure for *l*-InAs has been previously investigated,[5] its behavior is far from being fully understood due to the limited pressure range of the investigation ($2.3\ \mathrm{GPa} < P < 13.3\ \mathrm{GPa}$). This study extended the pressure range toward both the lower and higher pressure regions.

Furthermore, the *ab initio* molecular-dynamics simulation (AIMD) has been conducted to understand the pressure-induced evolution of the liquid structure. In a conventional x-ray diffraction technique, we cannot obtain the partial structure factors for liquid compounds, so we cannot know the chemical short-range order (CSRO) around each ion. To

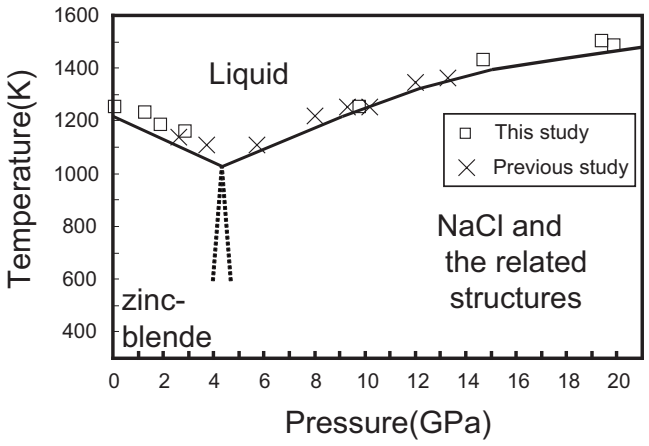

FIG. 1. *P-T* phase diagram of InAs and the experimental *P-T* condition. The melting curve is estimated from the results of this study. The dotted lines denote the uncertainty of the phase boundary due to the kinetic effect of the transformation.

reveal it is inevitable to fully understand pressure-induced structural changes of liquid compounds. On the other hand, the recent development of the computer simulation technique as well as the increase in the computation power enable us to calculate atomic and electronic structures of condensed matter precisely. In particular, the AIMD method is a powerful tool, and this method has been applied to many liquid compounds.[10–16] In this study, the AIMD simulation is conducted for *l*-InAs to understand experimentally observed pressure-induced evolution of the liquid structure.

II. EXPERIMENT

A. X-ray diffraction experiment

In addition to the pressure-temperature (*P-T*) conditions of our previous study,[5] the x-ray diffraction experiments were conducted at the conditions shown in Fig. 1. The data were collected by an energy-dispersive x-ray diffraction (EDX) method using a synchrotron radiation source. Two types of high-pressure apparatus were used in this study, depending on the pressure range. Below 13.3 GPa, we used a single-stage high-pressure apparatus, MAX80, which is installed on a bending magnet beamline, AR-NE5C at PF-AR at KEK. Above 14.7 GPa, we used a Kawai-type double-stage high-pressure apparatus, SPEED1500, which is installed in BL04B1 at SPring-8.[17] Reagent-grade 99.999% pure InAs (Rare Metallic Co., Ltd.) was mixed with the same materials as the container [NaCl or BN (Ref. 18)] to avoid heavy x-ray absorption. The cell assemblies used in the high-pressure experiments were nearly identical to those described in Refs. 19 and 20.

The pressure was determined from the lattice parameter of a pressure marker [NaCl or MgO (Ref. 21)] based on the equation of state.[22,23] The temperature was estimated from the electric power applied to the heater using the temperature–electric power relationship, which was determined beforehand. The respective estimated error in the pressure and temperature were within 0.7 GPa and 100 K below 6 GPa, and within 1.4 GPa and 200 K above 6 GPa.

The melting of the sample was judged from the disappearance of all the Bragg peaks and the simultaneous appearance of the halo pattern. The degeneration of the sample, such as the reaction to the sample container and the preferential evaporation of In or As, did not occur during the experiments. It was confirmed from the lack of significant changes in the x-ray diffraction pattern and the color of the recovered sample. The data were collected at several 2θ angles[24] to obtain $S(Q)$ over a wide Q region (at least up to $Q=15$ Å^{-1}). The $S(Q)$ was obtained by normalizing the diffraction profiles at several 2θ angles and connecting them to each other. The $g(r)$ was obtained by a Fourier transformation of $S(Q)$. Here, the $S(Q)$ and $g(r)$ are based on the Faber-Ziman definition.[25] The density of liquid under high *P-T* condition was estimated from the following three values: (i) the volume of the crystalline phase just before melting, (ii) the volume jump on melting,[26] and (iii) the thermal expansion of the liquid.[27] The error of the number density was considered to be within 5%. The detailed procedure is described in Ref. 4. The structural information of *l*-InAs is shown in Table I.

B. *Ab initio* molecular-dynamics simulation

The electronic structure calculations were performed using the projector-augmented-wave method[28,29] based on density functional theory within the generalized gradient approximation.[30] The plane-wave cutoff energies for the pseudo-wave-functions and the pseudo-electron-density were 11 and 70 Ry, respectively. The energy functional was minimized using an iterative scheme based on the preconditioned conjugate-gradient method.[31,32] The Γ point was used for the Brillouin zone sampling. A cubic supercell which contains 192 (96 In+96 As) atoms was used. The molecular-dynamics simulations were carried out at six thermodynamic states; the temperatures T (K) and number densities ρ (Å^{-3}) are $(T,\rho)=(1150,0.0348)$, (1100, 0.0395), (1100, 0.0420), (1350, 0.0452), (1450, 0.0479), and (1500, 0.0508). The pressures calculated for these states are 0.1, 3.0, 6.0, 10.6, 15.0, and 21.7 GPa, respectively. Using the Nosé-Hoover thermostat technique,[33,34] the equations of motion were solved via the explicit reversible integrators[35] with a time step of $\Delta t=3.1-3.6$ fs. The quantities of interest were obtained by averaging over about 12 ps after the initial equilibration, taking about 6 ps.

III. RESULTS

A. Total structure factor and total pair distribution function from x-ray diffraction experiments

Figure 2 shows the pressure dependence of the experimental $S(Q)$ for *l*-InAs. Near ambient pressure (0.1 GPa), $S(Q)$ has a hump on the high Q side of the first peak, which reflects the anisotropy of the local structure. Upon compression, all the peaks and the hump shift toward higher Q values. Simultaneously, the peaks become higher and the hump becomes smaller, which indicates that the anisotropy of the local structure becomes smaller as the pressure increases. However, the hump is observed at 19.9 GPa, suggesting that

TABLE I. Structural information for *l*-InAs at high pressures.

P (GPa)	Q_1 (Å^{-1})	Q_2 (Å^{-1})	Q_2/Q_1	$S(Q_1)$	$S(Q_2)$	r_1 (Å)	r_2 (Å)	r_2/r_1	CN Disordered[a]	CN Ordered[b]
0.1	2.29(1)	4.84(2)	2.12(1)	1.44	1.09	2.98(2)	6.32(3)	2.12(2)	5.9(3)	6.2(3)
1.3	2.30(1)	4.82(2)	2.09(1)	1.56	1.10	2.92(2)	6.17(3)	2.11(2)	5.8(3)	6.0(3)
1.9	2.31(1)	4.82(2)	2.09(1)	1.60	1.11	2.93(2)	6.14(3)	2.09(2)	6.2(3)	6.5(3)
2.6	2.32(1)	4.90(2)	2.11(1)	1.75	1.10	2.87(2)	6.05(3)	2.11(2)	6.1(2)	6.4(2)
2.9	2.33(1)	4.81(2)	2.06(1)	1.67	1.12	2.91(2)	6.04(3)	2.07(2)	5.9(3)	6.2(3)
3.7	2.34(1)	4.92(2)	2.10(1)	1.86	1.11	2.86(2)	5.98(3)	2.09(2)	6.1(2)	6.3(2)
5.7	2.38(1)	4.90(2)	2.06(1)	2.00	1.14	2.83(2)	5.86(3)	2.07(2)	6.1(2)	6.3(2)
8.0	2.40(1)	4.97(2)	2.07(1)	1.89	1.11	2.79(2)	5.82(3)	2.08(2)	5.8(2)	6.0(2)
9.3	2.40(1)	4.99(2)	2.08(1)	1.94	1.12	2.79(2)	5.79(3)	2.08(2)	5.9(2)	6.1(2)
9.8	2.43(1)	5.00(2)	2.06(1)	1.28	1.15	2.78(2)	5.71(3)	2.05(2)	6.4(2)	6.6(2)
10.2	2.41(1)	4.99(2)	2.07(1)	2.01	1.12	2.78(2)	5.74(3)	2.06(2)	6.2(2)	6.4(2)
12.0	2.45(1)	5.06(2)	2.07(1)	2.25	1.12	2.79(2)	5.69(3)	2.04(2)	7.0(2)	7.3(2)
13.3	2.46(1)	5.09(2)	2.07(1)	2.18	1.13	2.78(2)	5.69(3)	2.05(2)	6.7(2)	6.9(2)
14.7	2.48(1)	5.02(2)	2.02(1)	2.38	1.15	2.76(2)	5.58(3)	2.02(2)	7.1(2)	7.4(2)
19.4	2.54(1)	5.06(2)	1.99(1)	2.49	1.16	2.75(2)	5.48(3)	2.00(2)	7.5(2)	7.8(2)
19.9	2.54(1)	5.06(2)	1.99(1)	2.53	1.17	2.75(2)	5.45(3)	1.98(2)	7.5(2)	7.8(2)

[a]CN for the chemically disordered model is calculated assuming $g_{\mathrm{InIn}}=g_{\mathrm{AsAs}}=g_{\mathrm{InAs}}$.
[b]CN for the chemically ordered model is calculated assuming $g_{\mathrm{InIn}}=g_{\mathrm{AsAs}}=0$ in the first coordination shell.

the local structure is still anisotropic at that pressure.

When the pressure dependence is more carefully examined, a different dependence is observed below and above about 9 GPa. Below about 9 GPa, the second peak markedly shifts toward higher Q values, but at higher pressures, the shift becomes less prominent. The hump also behaves differently between the two pressure regions. Below about 9 GPa, the hump shifts toward a higher Q value along with a slight decrease in its height, but above about 9 GPa, the shift becomes less prominent and the height significantly decreases.

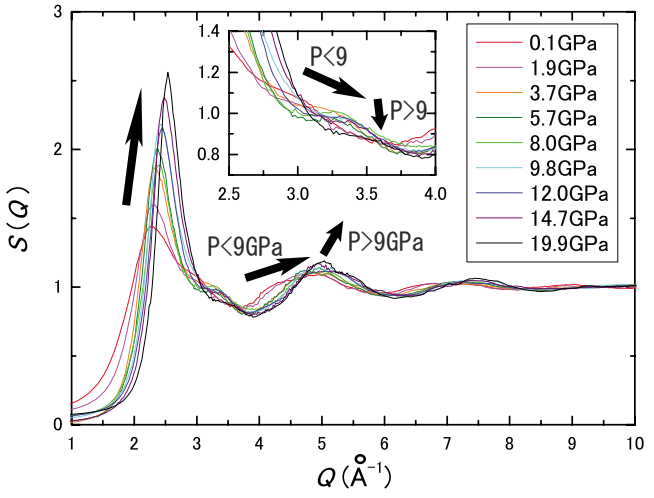

FIG. 2. (Color online) The $S(Q)$ of *l*-InAs at high pressures. To easily observe the pressure dependence, only the profile up to $Q=10$ Å^{-1} is shown. To generate $g(r)$, the data in the Q region up to 15 Å^{-1} are used.

The pressure dependence of the experimental $g(r)$ supports the change in the contraction behavior (Fig. 3). The profile changes its high-pressure behavior around 9 GPa. Namely, upon compression to about 9 GPa, the first minimum becomes deeper while maintaining the height of the hump, but at higher pressures, the depth remains almost unchanged and the hump markedly shifts toward the first peak. Furthermore, the second peak increases its height below 9 GPa, but the increase seems to stop at about 9 GPa. To more quantitatively show the change in the contraction behavior, the volume dependence of peak positions in $g(r)$ is shown in Fig. 4. Here, each value is normalized by the respective value at ambient pressure.[36] The figure shows that

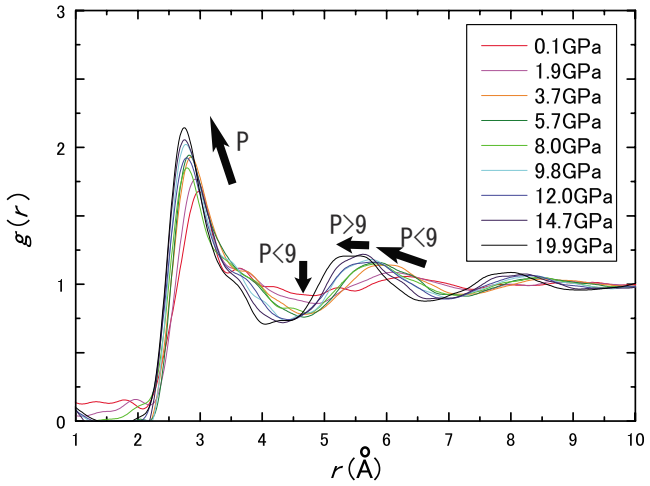

FIG. 3. (Color online) The $g(r)$ of *l*-InAs at high pressures.

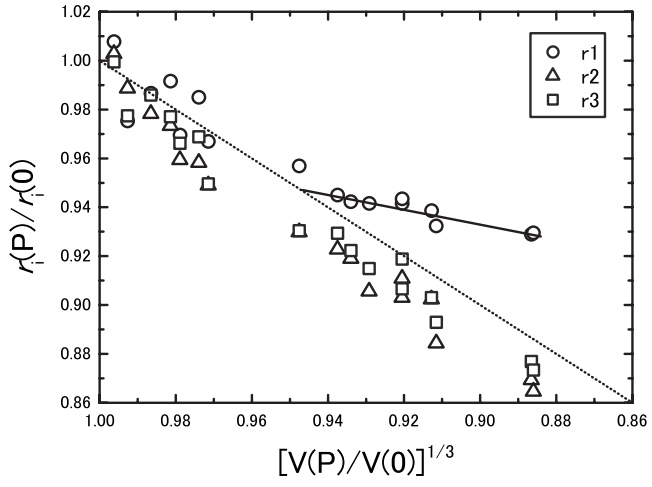

FIG. 4. Volume dependence of the peak positions in $g(r)$ for l-InAs. Each value is normalized by the respective one at ambient pressure. The dotted line represents the relationship expected for a uniform contraction. The solid line is only to guide the eyes.

as the volume decreases to $[V(P)/V(0)]^{1/3} \approx 0.94$, which corresponds to a compression up to about 9 GPa, all the peaks shift at the same rate, but at higher pressures, the first peak differently behaves from the others.

The pressure dependence of the average CN,[37] which is deduced from the experimental radial distribution function $[=4\pi r^2 \rho g(r)$, where ρ is the number density], also shows different behaviors below and above about 9 GPa. The pressure dependence of the experimental CN for l-InAs is shown in Fig. 5 and Table I. The CN remains constant up to about 9 GPa, but it starts to increase around 9 GPa.

B. Partial structure factors and partial pair distribution functions from the *ab initio* molecular-dynamics simulation

Figure 6(a) compares the total structure factors obtained by the AIMD calculation and the x-ray diffraction experiment. Throughout the entire pressure region, the calculation

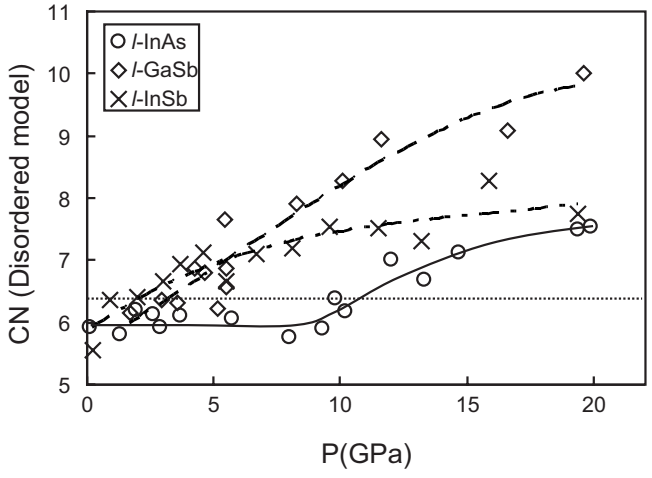

FIG. 5. Pressure dependence of the CN of l-InAs. Those for l-GaSb (Ref. 4) and l-InSb (Ref. 7) are also shown. Solid and dashed lines are only to guide the eyes. The dotted line is the criterion used to compare the $S(Q)$ of the three liquids in Fig. 12.

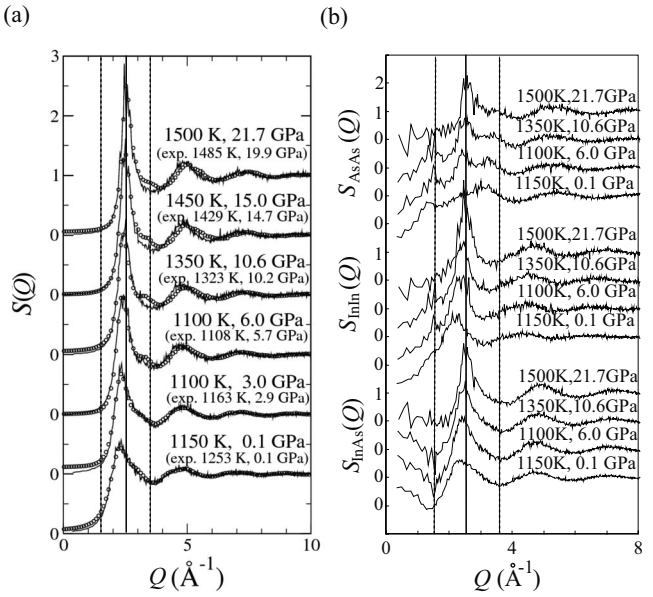

FIG. 6. (a) Total structure factors of l-InAs. The calculated results (solid lines) are compared with the experimental results (open circles). (b) The partial structure factors of l-InAs. Each structure factor is based on the Faber-Ziman definition (Ref. 25).

results agree with the experimental one in terms of position and height of the peaks, although the hump in the calculated $S(Q)$ is slightly lower than the experimental one.

Figure 6(b) shows the calculated partial structure factors $S_{ij}(Q)$ at high pressures. The first peak in the total structure factor around 2.5 Å^{-1} consists of all three correlations (In-In, As-As, and In-As). The correlation between like-ion pairs (As-As and In-In) and that for the unlike-ion pair (In-As) do not show the antiphase oscillation, suggesting that the chemical order is strongly destroyed in the liquid state despite the relatively large ionic chemical bonding character for InAs (Phillips ionicity,[38] f_i=0.357). On the other hand, the hump in $S(Q)$ around 3.5 Å^{-1} is mainly comprised of the As-As correlation, suggesting that the anisotropic feature of l-InAs is strongly related to the chemical bonding between As atoms. When the three correlations are more closely examined, it is found that the As-As correlation has a weak prepeak and the In-As correlation has a small dip around 1.5 Å^{-1}. However, no related peaks or dips are observed in the total $S(Q)$ due to their cancellation.

Upon compression, all three correlations change. For $S_{AsAs}(Q)$, the prepeak around 1.5 Å^{-1} disappears and a distinct peak appears around 2.5 Å^{-1}. However, the hump around 3.5 Å^{-1} is maintained even upon compression to 21.7 GPa, suggesting the persistence of the anisotropic local structures at such pressure. For $S_{InIn}(Q)$, the first peak near 2.5 Å^{-1} becomes more prominent and the slope at the low Q side of the first peak becomes steeper. Due to these changes, the profile more closely resembles that for a simple liquid metal. For the $S_{InAs}(Q)$, the first peak, which is relatively broad at 0.1 GPa, becomes sharper and higher, and the weak dip around 1.5 Å^{-1} disappears upon compression.

Figure 7(a) compares the total pair distribution functions obtained by the AIMD calculation and the x-ray diffraction

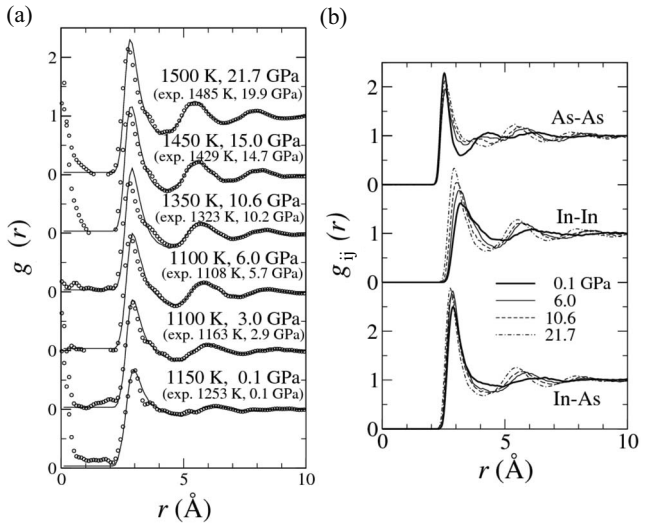

FIG. 7. (a) Total pair distribution functions of *l*-InAs. The calculated results (solid lines) are compared with the experimental results (open circles). (b) The partial pair distribution functions of *l*-InAs.

experiment. The calculation results agree well with the experimental ones, suggesting that we can discuss the pressure-induced evolution of the liquid structure based on the AIMD results. Figure 7(b) shows the pressure dependence of the partial pair distribution function $g_{ij}(r)$. The three profiles near ambient pressure (0.1 GPa) have various shapes, which reflects the different chemical bondings in each ion pair. In the $g_{\mathrm{AsAs}}(r)$ at 0.1 GPa, the second peak ($r \approx 4.2$ Å) is located relatively close to the first peak, and the first minimum is deeper than that for simple liquid metals. In the $g_{\mathrm{InAs}}(r)$ at 0.1 GPa, the first minimum is very shallow and the amplitudes of the second and third peaks are strongly dumped. On the other hand, the $g_{\mathrm{InIn}}(r)$ at 0.1 GPa shows a simple-liquid-metal-like profile, although the amplitude of the oscillation is much smaller.

Upon compression, the three $g_{ij}(r)$'s significantly change. In the $g_{\mathrm{AsAs}}(r)$, the second peak becomes less prominent, while the third peak becomes more prominent. Simultaneously, the first peak shifts toward a large r value despite compression. In the $g_{\mathrm{InAs}}(r)$, the fist minimum becomes deeper, while the severely dumped second and third peaks retain their height. Contrary to these, the $g_{\mathrm{InIn}}(r)$ shows a normal high-pressure behavior; upon compression, all the peaks shift toward small r values and the amplitude of the oscillation becomes larger. To compare the pressure dependence of the three correlations more quantitatively, the position of the first peak for each $g_{ij}(r)$, r_{ij}, is plotted as a function of the cube root of the specific volume $[V(P)/V(0)]^{1/3}$ (Fig. 8). Throughout the entire pressure region, the position is larger in the order of As-As, In-As, and In-In, which implies that the size of the first coordination shell is mainly controlled by the size of the constituent ions (the atomic radii that are defined by the half nearest neighbor distance in pure-element crystals are 1.62 Å for In and 1.25 Å for As at ambient pressure[39]). Upon compression, the first peaks of the three correlations change their high-pressure behaviors

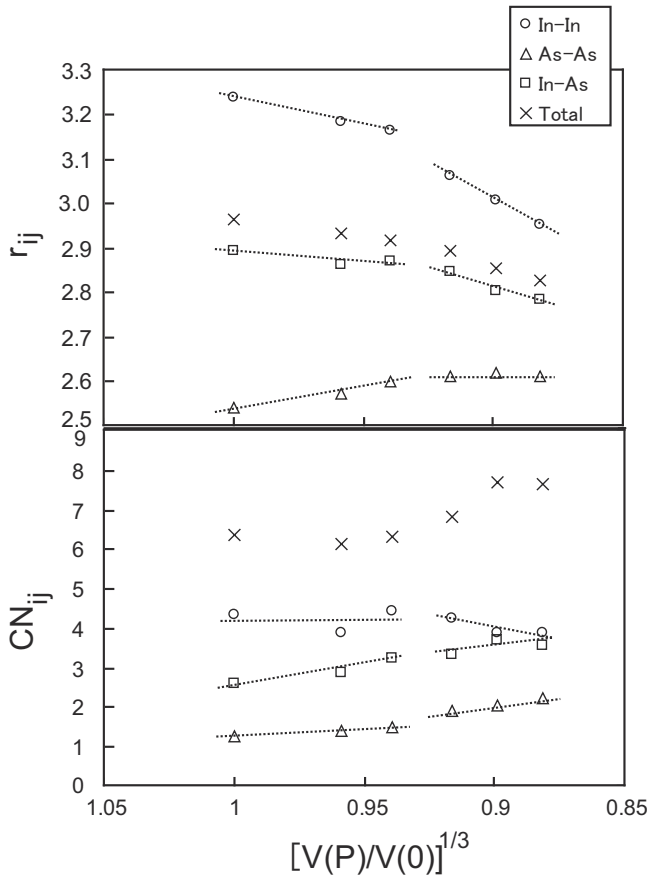

FIG. 8. First peak positions in $g_{ij}(r)$ (upper) and the CN_{ij} (lower) as a function of the cube root of the specific volume. Dotted lines are only to guide the eyes.

around $[V(P)/V(0)]^{1/3}=0.94$, which corresponds to a pressure of about 9 GPa. Namely, in the r_{InIn}, the rate of the decrease becomes larger above 9 GPa. In the r_{AsAs}, the interatomic distance increases up to 9 GPa, but it remains unchanged at higher pressures. The r_{InAs}, which is nearly constant below 9 GPa, decreases above 9 GPa. Corresponding to these changes, the partial coordination number CN_{ij} shows different pressure dependences below and above about 9 GPa. Among the three CN_{ij}'s, the $\mathrm{CN}_{\mathrm{AsAs}}$ most significantly changes; the $\mathrm{CN}_{\mathrm{AsAs}}$ remains nearly constant below 9 GPa, but increases at higher pressures. The pressure where the change in the contraction behavior is observed in the AIMD simulation agrees with that observed in x-ray diffraction experiments.

IV. DISCUSSION

A. Partial structure of *l*-InAs at ambient pressure

Before discussing the high-pressure behavior of *l*-InAs, the ambient structure is discussed based on the AIMD results. To understand the liquid structure, the results of *l*-GaSb, which is another typical III-V compound, may provide insight. In the past, Gu *et al.*[12] investigated the partial structures of *l*-GaSb by an AIMD simulation and showed that the partial pair distribution functions between like-ion

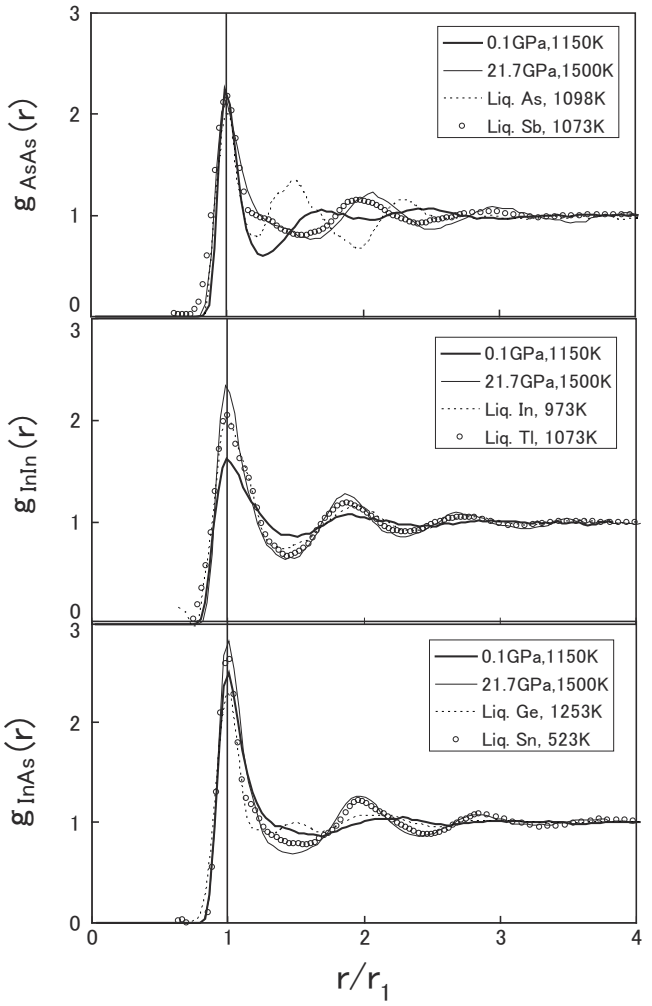

FIG. 9. Comparison of the $g_{ij}(r)$ with $g(r)$ for pure-element liquids. The $g(r)$ for *l*-As are from Ref. 45, and those for *l*-Sb, *l*-In, *l*-Tl, *l*-Ge, and *l*-Sn are from Ref. 50.

pairs [$g_{\mathrm{GaGa}}(r)$ and $g_{\mathrm{SbSb}}(r)$] resemble the $g(r)$ for the respective pure-element liquids [liquid Ga (*l*-Ga) and liquid Sb (*l*-Sb)]. To verify whether this is valid for *l*-InAs, the $g_{\mathrm{InIn}}(r)$ and the $g_{\mathrm{AsAs}}(r)$ were compared to the $g(r)$'s for liquid In (*l*-In) and liquid As (*l*-As), respectively (Fig. 9). In Fig. 9, the abscissa is scaled by the position of the first peak, taking the different sizes of the constituent ions into account. The $g(r)$'s for heavier elements in the same group are also shown in order to discuss the local structure of the high-pressure state later. The results show that, although the amplitude of the oscillation is much smaller, the profile shape of $g_{\mathrm{InIn}}(r)$ at 0.1 GPa is similar to that of *l*-In. The smaller amplitude is probably due to the interference of the shell structure for the In-In correlation by the other correlations (In-As and As-As). On the other hand, the profile of $g_{\mathrm{AsAs}}(r)$ at 0.1 GPa is not similar to that for *l*-As, unfortunately. However, the bond angle distribution suggests the existence of a liquid As-like local structure in *l*-InAs. Figure 10 shows the bond angle distribution $B_{\alpha\beta\gamma}(\theta)$ for various combinations of atoms.[40] The $B_{\mathrm{AsAsAs}}(\theta)$ at 0.1 GPa shows a maximum and a subsidiary peak around 100° and 60°, respectively. This distribution is nearly identical to those previously reported for *l*-As.[41–44]

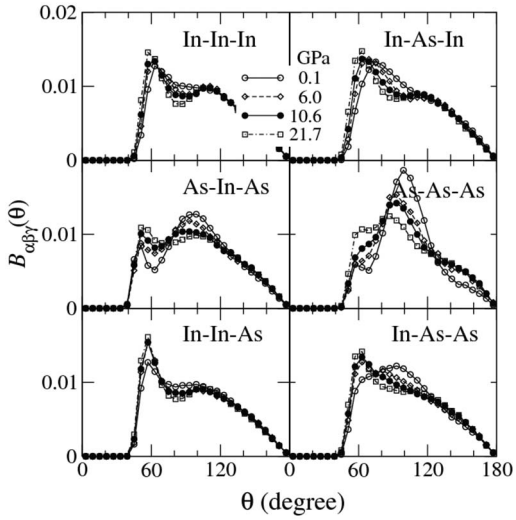

FIG. 10. Bond angle distribution $B_{\alpha\beta\gamma}(\theta)$ for various pairs of atoms. The θ is the angle between the two vectors from β atoms to α and γ atoms. The distribution is calculated for the configurations that satisfy the conditions, $r_{\mathrm{AsAs}}<3.0$ Å, $r_{\mathrm{InIn}}<3.5$ Å, and $r_{\mathrm{InAs}}<3.5$ Å.

By comparing with the *A*7 rhombohedral structure, the main peak at 100° is considered to originate from the ppσ bonding, which is slightly modified due to the Peierls distortion.[41–45] The similarity of the correlation of like-ion pair to that for a pure-element liquid is not only observed in *l*-InAs and *l*-GaSb but also for other liquids, such as InSb (Ref. 13) and CdTe.[14,46] Thus, the similarity may be generally observed in liquid compounds.

The above comparisons suggest the following view on the structure of liquid compounds. The lack of a complete CSRO causes a spatial fluctuation in the chemical composition. In a region where the composition largely deviates, like-ions form *wrong bonds*. In such regions, ions cannot form the same local structure as those realized in the crystalline state, which has a complete CSRO, due to the insufficient or excessive valence electrons. Instead, they form a local structure similar to that realized in a pure-element liquid. The view implies that the structure in liquid compounds is locally controlled by the number of the valence electrons in each ion pair. If this is true, then the In-As correlation in *l*-InAs should resemble those of liquids with four valence electrons, i.e., liquids of group 14 elements. To confirm this, the $g_{\mathrm{InAs}}(r)$ at 0.1 GPa is compared to that of liquid Ge (*l*-Ge) (Fig. 9). The results show that the two profiles have similar features; both profiles show a distinct first peak and subsequent strongly dumped oscillation. The bond angle distribution $B_{\mathrm{AsInAs}}(\theta)$ also shows similar features. The $B_{\mathrm{AsInAs}}(\theta)$ at 0.1 GPa shows a broad maxima around 100° in addition to the subsidiary peak around 50°, which agrees with the previously reported bond angle distribution for *l*-Ge.[31,47]

B. Pressure-induced change of the local structures in *l*-InAs

Next, let us examine the pressure-induced changes of the partial structures. Generally, the electron density increases

upon compression. Because heavier elements have larger electron densities, the structure of the compressed substances should resemble that of a heavier element. Actually, this is often observed in the high-pressure modifications of crystalline[48] and liquid states.[6,49] Therefore, each $g_{ij}(r)$ of l-InAs may approach the $g(r)$ for the liquid of a heavier element upon compression. To verify this, the partial $g_{\mathrm{InIn}}(r)$, $g_{\mathrm{AsAs}}(r)$, and $g_{\mathrm{InAs}}(r)$ at 21.7 GPa were compared to the $g(r)$'s for liquid Tl (l-Tl),[50] l-Sb,[50] and liquid Sn (l-Sn),[50] respectively (Fig. 9). Overall, all the profiles of $g_{ij}(r)$'s at 21.7 GPa are surprisingly similar to those for pure-element liquids of the heavier elements. More specifically, the profile for $g_{\mathrm{InIn}}(r)$ at 21.7 GPa has peaks and dips whose sizes are comparable to the respective ones for l-Tl. The positions of the maxima and minima also agree well with the respective ones for l-Tl. For the $g_{\mathrm{AsAs}}(r)$ at 21.7 GPa, in addition to the similarity in the position and height of all the peaks, the hump on the high Q side of the first peak ($r/r_1 \approx 1.25$) is also reproduced by the profile of l-Sb. In the $g_{\mathrm{InAs}}(r)$ at 21.7 GPa, the relatively shallow first minimum and subsequent dumped oscillation, which are mitigated upon compression but are still deviated from those for simple liquid metals, are successfully reproduced by the profile for l-Sn. These findings indicate that the $g_{ij}(r)$'s at high pressures resemble the $g(r)$'s of the corresponding pure-element liquids, and that the empirical rule that the high-pressure state is represented by the ambient state of a heavier element is valid for the partial structures of liquid compounds.

C. Systematic understanding of the pressure-induced structural changes of liquid III-V compounds

The pressure dependence of the structure of l-InAs is compared to those of other liquid III-V compounds (l-GaSb and l-InSb) to understand the pressure-induced structural changes of liquid III-V compounds systematically. Throughout this section, the systematics of the liquid structure are discussed based on the previously reported experimental results[4,7] because the pressure dependence of the partial structures for l-InSb is unobtainable at present.

Pressurization of liquids in group IV elements and III-V compounds causes a reduction in the covalent chemical bonding nature, which results in a decrease of the anisotropy in the local structures. Therefore, the pressure dependence of the structural parameters that are sensitive to the anisotropy is compared among three liquid III-V compounds. Figure 11 compares the pressure dependence of the position of the second peak relative to that for the first peak in $S(Q)$, Q_2/Q_1. The three liquids appear to have similar sequences. The ratio near ambient pressure is about 2.10–2.15. This ratio gradually decreases upon compression and the rate of the decrease is relatively large in the region where the ratio is between 2.05 and 1.95. These observations imply that the pressure dependence of the three liquids can be explained by a common sequence. That is, shifting the pressure-Q_2/Q_1 relation curves for l-InAs and l-GaSb toward a lower pressure causes the pressure dependence of the three liquids to lie on an identical curve. This shift is reasonable considering the parallelism between the pressurization and the chemical substitution by a heavy element and the larger average atomic number for InSb (Z=50) than those for GaSb (Z=41) and InAs (Z=41). To confirm this common sequential change, the pressure dependences of the average CN of the three liquids are compared (Fig. 5). The l-InAs has the smallest value at ambient pressure, which gradually increases above 9 GPa. For l-GaSb, the corresponding increase seems to begin between 2 and 4 GPa. The l-InSb also shows a corresponding increase at 0.9 GPa. These findings support the hypothesis that the pressure-induced structural changes in the three liquids are explained by a common structural change. In addition, the pressure dependence of the $S(Q)$ of the three liquids also supports this idea. Figure 12 compares the $S(Q)$ profiles of the three liquids at a pressure where the CN is about 6.4. Here, the abscissa is scaled by the position of the first peak, Q_1, considering the size difference of the constituent atoms. Although each liquid shows a marked pressure-induced change in its profiles, such as increased peak, decreased hump heights, and a decreased Q_2/Q_1 ratio,[4,7] the three $S(Q)$ profiles, which are selected by the above criterion, are found to resemble one another in terms of not only the peak positions but also their heights. This finding also supports that the three liquids show the identical pressure-induced evolution of the local structure. Together with the calculation results, this behavior can be understood as follows. The local structure of liquid compounds consists of the three correlations, and each correlation has a parallelism between pressurization and the chemical substitution by a heavy element. Therefore, the average structures [total $S(Q)$, $g(r)$] or structural parameters obtained from them would also show good correspondence, although the corresponding state appears at different pressures.

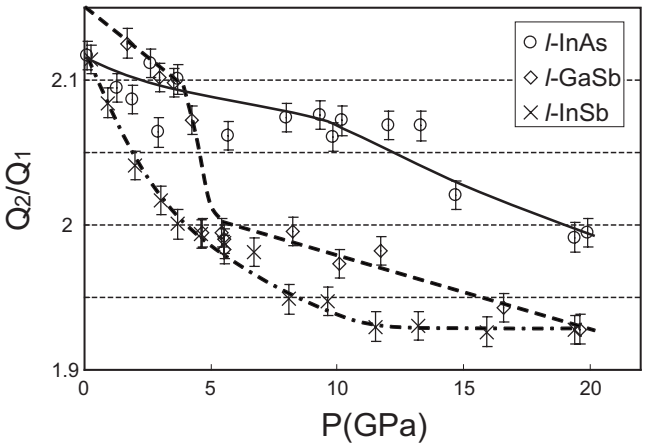

FIG. 11. Comparison of the pressure dependence of the Q_2/Q_1 ratio among the liquid III-V compounds. Data of l-GaSb and l-InSb are from Refs. 4 and 7, respectively. The lines are only to guide the eyes.

When the pressure-induced structural changes of the three liquids are understood by the common structural sequence, a strong correlation is expected between the structural parameters sensitive to the structural change, regardless of pressure. To reveal this correlation, Fig. 13 plots the relationship between the Q_2/Q_1 ratio and the CN of the three liquids. The

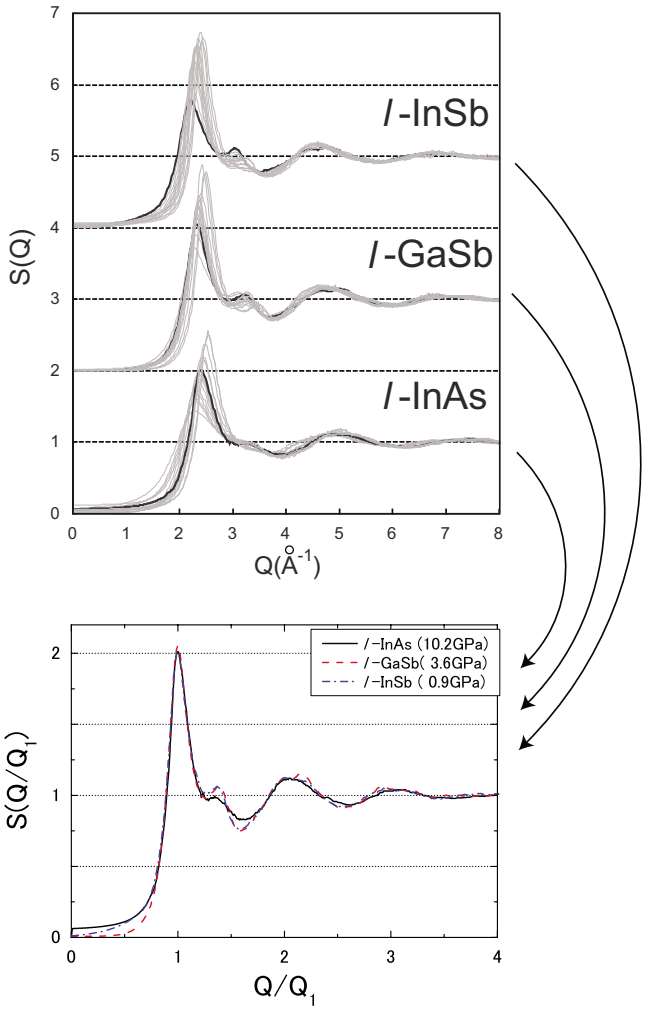

FIG. 12. (Color online) Comparison of $S(Q)$ of liquid III-V compounds. The $S(Q)$ at a pressure where the CN is about 6.4 shown. Data of *l*-GaSb and *l*-InSb are from Refs. 4 and 7, respectively.

figure reveals a strong correlation between the two parameters despite differing pressure values. This also implies that the structural parameters sensitive to anisotropy in the local structure become good parameters to scale the pressure-induced structural change of liquid III-V compounds.

D. Comparison of the pressure-induced structural changes to those in the crystalline counterparts

As already mentioned, increasing atomic number and the pressurization give similar effects, and this empirical rule is applicable to the pressure-induced structural changes in liquid III-V compounds (GaSb, InSb, and InAs). This is reasonable because, in tetrahedrally bonded materials, the empirical rule is based on a decrease of the covalent chemical bonding nature due to the increase in the electron density, which is caused by compression or by an increase in the average atomic number. This effect is substantially common in both crystalline and liquid states, and it is plausible that the same behavior is observed for high-pressure transitions in crystalline III-V compounds. However, the actual pressure-induced structural changes for the crystalline states do not show such behavior. Namely, crystalline GaSb and InSb transform from the zinc blende phase into a metallic phase with partial covalent bonding such as the β-tin and/or related phases (orthorhombic *Imma*, *Immm*, and super-*Cmcm* phases),[51,52] but crystalline InAs transforms from the zinc blende phase into an ionic phase such as NaCl and the related orthorhombic *Cmcm* phase.[51,52] The different behavior in crystalline states from that in liquid states is related to the chemical short-range order and its effect on the pressure-induced structural changes.

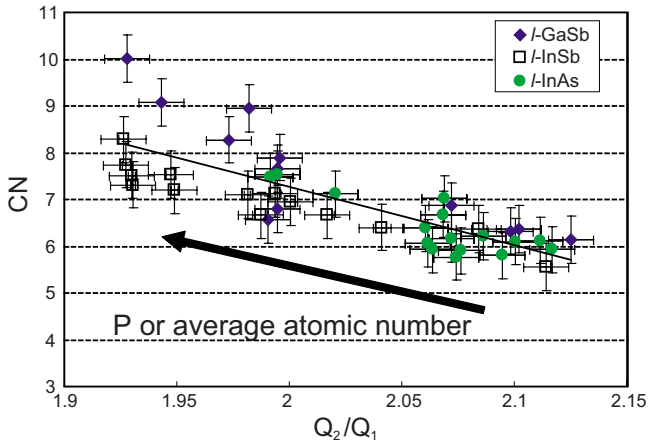

FIG. 13. (Color online) Relationship between the Q_2/Q_1 ratio and the CN. The thin line is the linear fit result. Data for GaSb and InSb are from Refs. 4 and 7, respectively.

V. CONCLUSION

To understand the pressure-induced structural changes of liquid III-V compounds systematically, the pressure dependence of *l*-InAs was investigated using the synchrotron x-ray diffraction and an *ab initio* molecular-dynamics simulation. The results are summarized as follows:

(i) The x-ray diffraction experiments have revealed that the liquid changes its compression behavior from a nearly uniform type into a nonuniform one around 9 GPa. Corresponding to this change, the coordination number (CN) which is maintained up to 9 GPa, markedly increases from 6.0 to 7.5. The AIMD simulation has revealed that this change is related to the change in the pressure dependence of all three pair correlations. In particular, a marked change is observed in the As-As correlation; in the low-pressure region, the position of the first peak in $g_{\mathrm{AsAs}}(r)$, r_{AsAs}, increases while maintaining the $\mathrm{CN}_{\mathrm{AsAs}}$, but in the high-pressure region, the r_{AsAs} stops increasing and the $\mathrm{CN}_{\mathrm{AsAs}}$ begins to increase.

(ii) The AIMD simulation has also revealed that each partial structure of *l*-InAs is similar to that for a pure-element liquid with the same valence electron number. Upon compression, each partial structure approaches the respective one for a heavier element in the same group. These findings suggest that the structure of the liquid compounds is locally

controlled by the number of the valence electrons in each ion pair and that the change in each partial structure obeys the empirical rule that the high-pressure state resembles the ambient state of the heavy element in the same group.

Furthermore, comparing the pressure-induced structural change of *l*-InAs to those for other liquid III-V compounds (GaSb and InSb) indicates that, although the high-pressure behaviors of these three liquids are apparently different, their structural changes are systematically understood by a common structural sequence, which originates from the same effect on each partial structure between increasing the atomic number and the pressurization.

ACKNOWLEDGMENTS

We thank N. Funamori, T. Kikegawa, K. Funakoshi, and W. Utsumi for their support in the experiments. The work was performed with the approvals of the Photon Factory Program Advisory Committee (Proposals No. 2000G044 and No. 2002G049) and the Japan Synchrotron Radiation Research Institute (JASRI) (Proposal No. 2002B0143-CD2-np).

*takanori@spring8.or.jp

[1] N. Funamori and K. Tsuji, Phys. Rev. Lett. **88**, 255508 (2002).
[2] T. Mori, M.S. thesis, Keio University, 2000.
[3] J. Kōga, H. Okumura, K. Nishio, T. Yamaguchi, and F. Yonezawa, Phys. Rev. B **66**, 064211 (2002).
[4] T. Hattori, K. Tsuji, N. Taga, Y. Takasugi, and T. Mori, Phys. Rev. B **68**, 224106 (2003).
[5] T. Hattori, T. Kinoshita, T. Narushima, and K. Tsuji, J. Phys.: Condens. Matter **16**, S997 (2004).
[6] K. Tsuji, T. Hattori, T. Mori, T. Kinoshita, T. Narushima, and N. Funamori, J. Phys.: Condens. Matter **16**, S989 (2004).
[7] T. Hattori, T. Kinoshita, N. Taga, Y. Takasugi, T. Mori, and K. Tsuji, Phys. Rev. B **72**, 064205 (2005).
[8] T. Kinoshita, T. Hattori, T. Narushima, and K. Tsuji, Phys. Rev. B **72**, 060102(R) (2005).
[9] T. Hattori, T. Kinoshita, T. Narushima, K. Tsuji, and Y. Katayama, Phys. Rev. B **73**, 054203 (2006).
[10] Q. M. Zhang, G. Chiarotti, A. Selloni, R. Car, and M. Parrinello, Phys. Rev. B **42**, 5071 (1990).
[11] V. Godlevsky and J. R. Chelikowsky, J. Chem. Phys. **109**, 7312 (1998).
[12] T. Gu, J. Qin, X. Bian, C. Xu, and Y. Qi, Phys. Rev. B **70**, 245214 (2004).
[13] T. Gu, X. Bian, J. Qin, and C. Xu, Phys. Rev. B **71**, 104206 (2005).
[14] V. V. Godlevsky, J. J. Derby, and J. R. Chelikowsky, Phys. Rev. Lett. **81**, 4959 (1998).
[15] F. Shimojo, M. Aniya, and K. Hoshino, J. Phys. Soc. Jpn. **73**, 2148 (2004).
[16] T. Gu, J. Qin, X. Bian, and C. Xu, J. Chem. Phys. **125**, 094506 (2006).
[17] W. Utsumi, K. Funakoshi, S. Urakawa, Y. Yamakata, K. Tsuji, H. Konishi, and O. Shimomura, Rev. High Pressure Sci. Technol. **7**, 1484 (1998).
[18] In the *P-T* region where rocksalt melts, boron nitride was used as a sample container.
[19] K. Tsuji, K. Yaoita, M. Imai, O. Shimomura, and T. Kikegawa, Rev. Sci. Instrum. **60**, 2425 (1989).
[20] N. Funamori and K. Tsuji, Phys. Rev. B **65**, 014105 (2001).
[21] In the *P-T* region where rocksalt melts, magnesia was used as a pressure marker.
[22] D. L. Decker, J. Appl. Phys. **42**, 3239 (1971).
[23] J. C. Jamieson, J. N. Fritz, and M. H. Manghani, *High Pressure Research in Geophysics* (Center for Academic Publications, Tokyo, 1982).
[24] The diffraction profiles were taken at $2\theta=3°$, 4°, 5°, 6°, 8°, 10°, 12°, 15°, and 20° for the experiments at PF-AR, and at $2\theta=3°$, 4°, 5°, 6°, 8°, 11°, and 15° for the experiments at SPring-8.
[25] T. E. Faber and J. M. Ziman, Philos. Mag. **11**, 153 (1965).
[26] We estimated the volume jump on melting at high pressures from that at ambient pressure and the slope of the melting curve on the basis of the Clausius-Clapeyron relation. Here, we assumed that the entropy change on melting is independent of pressure in the pressure range of the present study.
[27] The thermal expansion coefficient of the liquid was assumed to be equal to that of the crystalline phase before melting at each pressure. The error caused by this assumption is negligibly small because the contribution of the thermal expansion to the number density is small (within 1%).
[28] G. Kresse and D. Joubert, Phys. Rev. B **59**, 1758 (1999).
[29] P. E. Blöchl, Phys. Rev. B **50**, 17953 (1994).
[30] J. P. Perdew, K. Burke, and M. Ernzerhof, Phys. Rev. Lett. **77**, 3865 (1996).
[31] G. Kresse and J. Hafner, Phys. Rev. B **49**, 14251 (1994).
[32] F. Shimojo, R. K. Kalia, A. Nakano, and P. Vashishta, Comput. Phys. Commun. **140**, 303 (2001).
[33] S. Nosé, Mol. Phys. **52**, 255 (1984).
[34] W. G. Hoover, Phys. Rev. A **31**, 1695 (1985).
[35] M. Tuckerman, B. J. Berne, and G. J. Martyna, J. Chem. Phys. **97**, 1990 (1992).
[36] The values at ambient pressure are estimated by interpolating the data in the low-pressure region, where the parameters show linear response to pressure, toward ambient pressure.
[37] In binary liquids, four partial coordination numbers, CN_{AA}, CN_{AB}, CN_{BA}, and CN_{BB}, are defined (the CN_{AB} and CN_{BA} become identical when a compound has a chemical composition of $A_{0.5}B_{0.5}$). Here, each CN_{ij} represents the number of *j*-type atoms around an *i*-type atom. Because a conventional EDX method does not produce these numbers, the average CN was calculated assuming two states with different chemical short-range ordering, i.e., a completely ordered state and a completely disordered one (Ref. 4).
[38] J. C. Phillips, *Bonding and Bands in Semiconductors* (Academic, New York, 1973).
[39] R. Kiriyama and H. Kiriyama, *Kouzoumukikagaku I* (Kyouritsu Shuppan, Tokyo, 1964).
[40] In the calculation, the following cutoff distances are adopted: $r^c_{\mathrm{AsAs}}=3.0$ Å, $r^c_{\mathrm{InIn}}=3.5$ Å, and $r^c_{\mathrm{InAs}}=3.5$ Å. Each cutoff distance

covers most part of the first coordination shell for the individual $g_{ij}(r)$.

[41] J. Hafner, Phys. Rev. Lett. **62**, 784 (1989).

[42] J. Hafner and W. Jank, Phys. Rev. B **45**, 2739 (1992).

[43] C. Bichara, A. Pellegatti, and J. P. Gaspard, Phys. Rev. B **47**, 5002 (1993).

[44] X. P. Li, Phys. Rev. B **41**, 8392 (1990).

[45] R. Bellissent, C. Bergman, R. Ceolin, and J. P. Gaspard, Phys. Rev. Lett. **59**, 661 (1987).

[46] V. V. Godlevsky, M. Jain, J. J. Derby, and J. R. Chelikowsky, Phys. Rev. B **60**, 8640 (1999).

[47] N. Takeuchi and I. L. Garzon, Phys. Rev. B **50**, 8342 (1994).

[48] D. A. Young, *Phase Diagrams of The Elements* (University of California Press, Berkeley, 1991).

[49] Y. Katayama and K. Tsuji, J. Phys.: Condens. Matter **15**, 6085 (2003).

[50] Y. Waseda, *The Structure of Non-Crystalline Materials* (McGraw-Hill, New York, 1980).

[51] R. J. Nelmes and M. I. McMahon, Semicond. Semimetals **54**, 145 (1998).

[52] A. Mujica, A. Rubio, A. Munoz, and R. J. Needs, Rev. Mod. Phys. **75**, 863 (2003).